iScience

CellPress
OPEN ACCESS

Article

Regulation of splenic monocyte homeostasis and function by gut microbial products

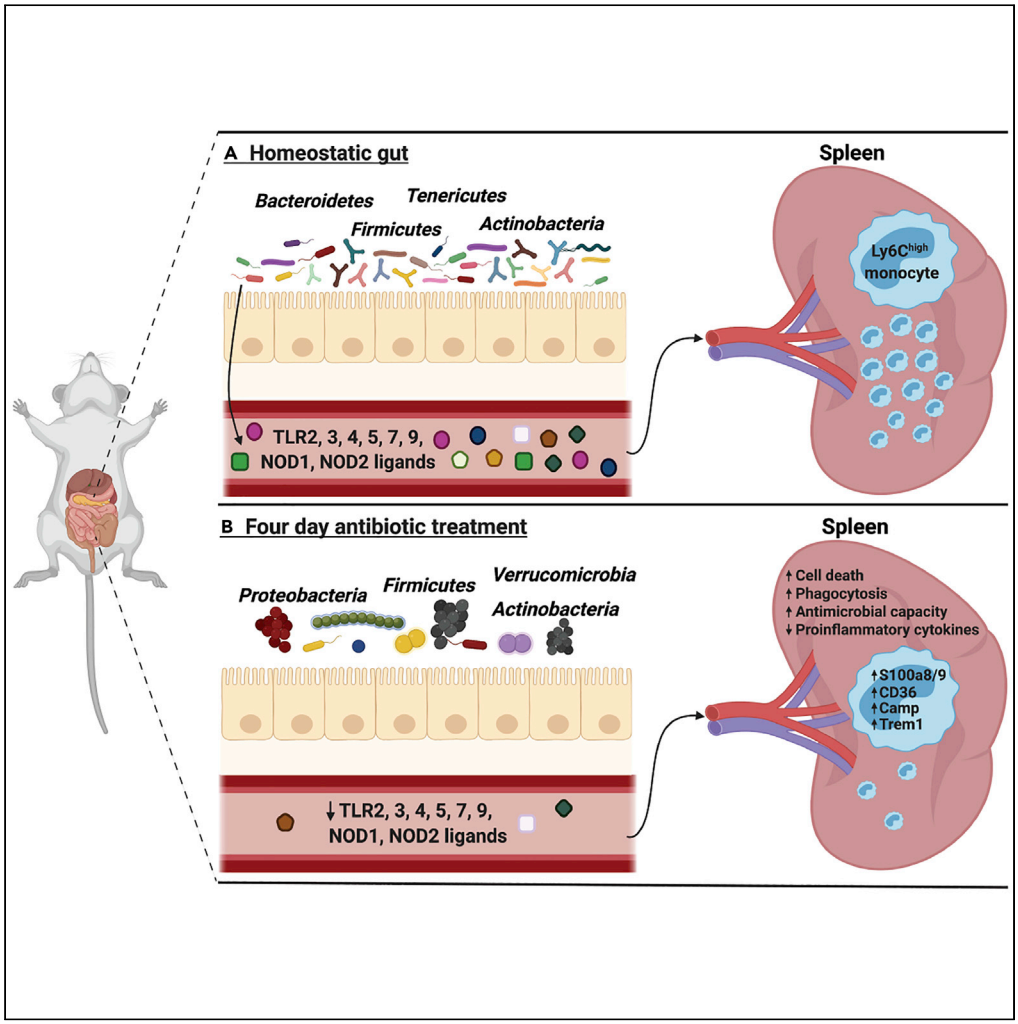

Panayota Kolypetri, Shirong Liu, Laura M. Cox, ..., Dominique Daatselaar, Valerie Willocq, Howard L. Weiner

hweiner@rics.bwh.harvard.edu

Highlights

A 4-day antibiotic treatment eliminates certain bacterial families in the gut

Gut dysbiosis is followed by reduced levels of PRR ligands in the circulation

Reduction of PRR ligands relates to perturbation of splenic Ly6C^{high} monocytes

Addition of PRR ligands restores splenic Ly6C^{high} monocyte numbers and function

Kolypetri et al., iScience 24, 102356
April 23, 2021 © 2021 The Authors.
https://doi.org/10.1016/j.isci.2021.102356

iScience

CellPress
OPEN ACCESS

Article

Regulation of splenic monocyte homeostasis and function by gut microbial products

Panayota Kolypetri,[1,2] Shirong Liu,[1,2] Laura M. Cox,[1,2] Mai Fujiwara,[1,2] Radhika Raheja,[1,2] Dvora Ghitza,[1,2] Anya Song,[1,2] Dominique Daatselaar,[1,2] Valerie Willocq,[1,2] and Howard L. Weiner[1,2,3,*]

SUMMARY

Splenic Ly6C^{high} monocytes are innate immune cells involved in the regulation of central nervous system-related diseases. Recent studies have reported the shaping of peripheral immune responses by the gut microbiome via mostly unexplored pathways. In this study, we report that a 4-day antibiotic treatment eliminates certain families of the Bacteroidetes, Firmicutes, Tenericutes, and Actinobacteria phyla in the gut and reduces the levels of multiple pattern recognition receptor (PRR) ligands in the serum. Reduction of PRR ligands was associated with reduced numbers and perturbed function of splenic Ly6C^{high} monocytes, which acquired an immature phenotype producing decreased levels of inflammatory cytokines and exhibiting increased phagocytic and anti-microbial abilities. Addition of PRR ligands in antibiotic-treated mice restored the number and functions of splenic Ly6C^{high} monocytes. Our data identify circulating PRR ligands as critical regulators of the splenic Ly6C^{high} monocyte behavior and suggest possible intervention pathways to manipulate this crucial immune cell subset.

INTRODUCTION

The gut microbiome has recently emerged as a key regulator of the peripheral innate immunity as well as myelopoiesis in the bone marrow (BM) (Belkaid and Harrison, 2017). At steady state, gut microbiome-derived products and metabolites cross the intestinal barrier and enter the bloodstream affecting the differentiation potential of BM precursor cells (Khosravi et al., 2014; Balmer et al., 2014) as well as the function of innate immune cells in peripheral tissues (Gorjifard and Goldszmid, 2016). Microbial peptidoglycan fragments have been reported to be present in the sera and BM of naive mice regulating the anti-microbial ability of BM-derived neutrophils (Clarke et al., 2010). Also, the bacteria-derived lipodipeptide, lipid 654, a Toll-like receptor (TLR) 2 ligand, is present in the serum of healthy individuals, but its levels are significantly decreased in patients with multiple sclerosis (Farrokhi et al., 2013), whereas its administration at low levels in mice attenuates experimental autoimmune encephalomyelitis (EAE) (Anstadt et al., 2016). Recently, the muramyl dipeptide (MDP), a NOD2 ligand, was found to be ubiquitously present in the sera of healthy humans, mice, and monkeys and was reported to participate in the immunoregulation of autoimmune arthritis and EAE (Huang et al., 2019). Another major group of microbial metabolites regulating the peripheral innate immune responses are short-chain fatty acids (SCFAs), products of fermentation of indigestible dietary fibers in the cecum and colon (Kim, 2018). The aforementioned findings demonstrate that in the absence of infection, there is a continuous communication between the gut microbiota and peripheral innate cells mediated by circulating microbial signals. Perturbation of this cross talk affects peripheral autoimmune processes and disease development.

Among peripheral innate immune cells, splenic-resident Ly6C$^{high/low}$ monocytes play a prominent immunoregulatory role under inflammatory conditions as they are mobilized and rapidly recruited to injured tissues (Guilliams et al., 2018). During the onset of EAE, splenic Ly6C^{high} monocytes acquire an immunosuppressive function (Zhu et al., 2007), which they maintain within the central nervous system (CNS) as they express *Nos2* and *Arg1*, hallmark genes of myeloid-derived suppressor cells (Zhu et al., 2007; Giladi et al., 2020). Their abundance has recently been related to a milder EAE course (Melero-Jerez et al., 2020). Splenic Ly6C^{high} monocytes are also involved in the regulation of amyotrophic lateral sclerosis (ALS) because they acquire an M1 signature before disease onset and treatment with an anti-Ly6C monoclonal antibody leads to reduced monocyte recruitment to the spinal cord, diminished neuronal loss, and extended survival in mice (Butovsky et al., 2012). Furthermore, splenic Ly6C^{high} monocytes regulate the acute and post-acute

[1]Department of Neurology, Ann Romney Center for Neurologic Diseases, Brigham and Women's Hospital, Harvard Medical School, Boston, MA 02115, USA

[2]Evergrande Center for Immunologic Diseases, Brigham and Women's Hospital, Harvard Medical School, Boston, MA 02115, USA

[3]Lead contact

*Correspondence: hweiner@rics.bwh.harvard.edu

https://doi.org/10.1016/j.isci.2021.102356

This is an open access article under the CC BY-NC-ND license (http://creativecommons.org/licenses/by-nc-nd/4.0/).

phases of spinal cord injury since prevention of early monocyte infiltration has been associated with improved disease recovery (Blomster et al., 2013). These studies highlight the regulatory function of splenic monocytes during the development of CNS-related diseases and demonstrate the need to further understand their biology.

In this study, we investigated the premise that the gut microbiome generates and secretes pattern recognition receptor (PRR) ligands in the circulation that regulate splenic Ly6C^{high} monocyte homeostasis and function at steady state. We performed a 4-day antibiotic treatment to perturb the gut microbiome and simultaneously avoid impairment of hematopoiesis in the BM (Josefsdottir et al., 2017) that is known to affect myeloid cell populations in the spleen (Khosravi et al., 2014). We profiled immediate changes in the levels of several circulating PRR ligands and in the number and function of splenic-resident Ly6C^{high} monocytes. Our findings (1) considerably expand the number of known PRR ligands present in the circulation at steady state and (2) demonstrate the role of PRR ligands in modulating the splenic Ly6C^{high} monocyte immune profile during steady state.

RESULTS

Families of the Bacteroidetes, Firmicutes, Tenericutes, and Actinobacteria phyla are the most susceptible taxa to our antibiotic treatment

To investigate whether the gut microbiome has a regulatory role on the splenic monocyte homeostasis and function, we initiated our study by treating C57BL/6 mice with a broad-spectrum antibiotic cocktail for 4 days to disturb the gut microbiome. A significant decrease in bacterial abundance was detected in fecal samples 2 and 4 days post antibiotic administration (Figure 1A). Bacterial composition was significantly changed at the levels of alpha (measured by Shannon's index and observed operational taxonomic units) and beta (measured by unweighted and weighted UniFrac analysis) diversity 2 and 4 days post antibiotic administration (Figures 1B and 1C, and S1). Taxonomic analysis using the linear discriminant analysis effect size (LEfSe) algorithm showed a significant decrease in the relative abundance of Bacteroidetes, Firmicutes, Tenericutes, and Actinobacteria with a concomitant increase in Proteobacteria in the antibiotic-treated group (Figures 1D and 1F). Among the most affected taxa were members of the S24_7 and Rikenellaceae families of the Bacteroidetes phylum because their relative abundance was shifted from 40.71% to 1.1% and 0.49% and from 20.6% to 2.58% and 1.14%, respectively, during treatment (Figures 1E and 1G and Tables S1 and S2). Within the Firmicutes phylum, several members of the Clostridiaceae, Lachnospiraceae, Ruminococcaceae, and Mogibacteriaceae families underwent a significant decrease, whereas a modest reduction was detected for Mollicutes RF39, Tenericutes phylum, and Bifidobacterium, Actinobacteria phylum, in the treated group. Overall, our data describe significant quantitative and qualitative changes in the homeostasis of the gut microbiota after 2 and 4 days of antibiotic treatment and identify certain families of the Bacteroidetes, Firmicutes, Tenericutes, and Actinobacteria phyla as the most susceptible bacterial taxa to our treatment.

Decreased levels of PRR ligands in the circulation and perturbation of the splenic monocyte homeostasis upon dysbiosis of the gut microbiota

We next addressed whether dysbiosis of the gut microbiota affected the levels of microbial products in the circulation of antibiotic-treated animals. Mice were administered drinking water with (n = 7) or without (n = 4) antibiotics, and sera were collected before (day 0) and on days 2 and 4 of treatment. Detection of PRR ligands in the sera of individual mice was tested using the HEK-Blue PRR reporter cell lines. Ligands for TLR2, 3, 4, 5, 7, and 9 and NOD1 and 2 were constitutively present at low levels on day 0 in all mice from both groups (Figures 2A and 2B). By day 4, the levels of all PRR ligands were significantly decreased only in mice receiving antibiotic treatment, suggesting (1) that the gut microbiome is the source producing and secreting PRR ligands into the circulation at steady state and (2) that a brief exposure to antibiotics was sufficient to mediate this reduction in PRR ligand levels.

To examine whether the reduction in the levels of PRR ligands would correlate with changes in the splenic monocyte homeostasis, we analyzed the frequency and absolute numbers of Ly6C^{high} monocytes in the spleens of mice treated with or without antibiotics for 2, 4, and 6 days. Both the frequency and absolute numbers of splenic Ly6C^{high} monocytes were significantly decreased in the experimental group after 4 and 6 days of antibiotic treatment compared with the untreated mice (Figure 2C). Similar observations were not detected in the BM of the same animals (Figure 2D) suggesting that the short-term antibiotic treatment did not impair hematopoiesis in the BM, known to affect the numbers of splenic monocytes

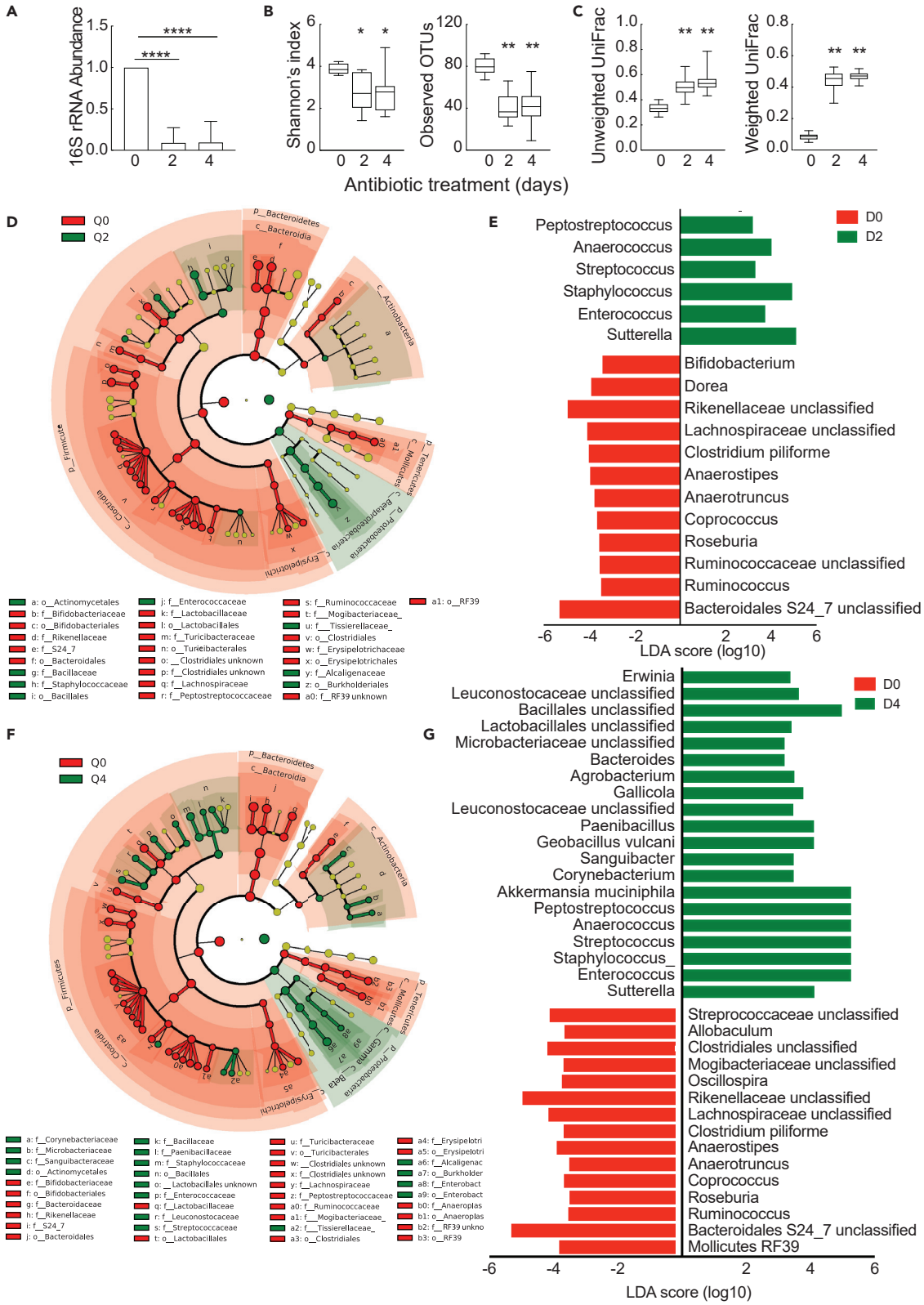
A
16S rRNA Abundance
****
****
B
Shannon's index
Observed OTUs
C
Unweighted UniFrac
Weighted UniFrac
Antibiotic treatment (days)
D
Q0
Q2
E
D0
D2
Peptostreptococcus
Anaerococcus
Streptococcus
Staphylococcus
Enterococcus
Sutterella
Bifidobacterium
Dorea
Rikenellaceae unclassified
Lachnospiraceae unclassified
Clostridium piliforme
Anaerostipes
Anaerotruncus
Coprococcus
Roseburia
Ruminococcaceae unclassified
Ruminococcus
Bacteroidales S24_7 unclassified
LDA score (log10)
F
Q0
Q4
G
D0
D4
Erwinia
Leuconostocaceae unclassified
Bacillales unclassified
Lactobacillales unclassified
Microbacteriaceae unclassified
Bacteroides
Agrobacterium
Gallicola
Leuconostocaceae unclassified
Paenibacillus
Geobacillus vulcani
Sanguibacter
Corynebacterium
Akkermansia muciniphila
Peptostreptococcus
Anaerococcus
Streptococcus
Staphylococcus_
Enterococcus
Sutterella
Streprococcaceae unclassified
Allobaculum
Clostridiales unclassified
Mogibacteriaceae unclassified
Oscillospira
Rikenellaceae unclassified
Lachnospiraceae unclassified
Clostridium piliforme
Anaerostipes
Anaerotruncus
Coprococcus
Roseburia
Ruminococcus
Bacteroidales S24_7 unclassified
Mollicutes RF39
LDA score (log10)

Figure 1. Families of the Bacteroidetes, Firmicutes, Tenericutes, and Actinobacteria phyla are the most susceptible taxa to our antibiotic treatment

(A) Relative expression of 16S rRNA in fecal samples of mice drinking water with or without antibiotics for 2 and 4 days. Quantification was performed using qPCR analysis. Relative expression was normalized to milligrams of fecal sample. Data represent mean ± SD, n = 8.

(B) Shannon's entropy index and observed OTUs were calculated for fecal microbial communities to compare differences in alpha-diversity between samples from antibiotic-treated and untreated animals for the indicated time period. Statistical significance was calculated using the Kruskal-Wallis pairwise test.

(C) Beta-diversity values were calculated using the unweighted and weighted UniFrac distance, to examine differences in overall microbial communities. Statistical significance was calculated using the PERMANOVA pair wise test.

(D) Taxonomic cladogram obtained from LEfSe analysis of 16S sequences from fecal samples of antibiotic-treated and untreated animals. Red color indicates the bacterial taxa enriched in untreated animals (Q0), whereas green color indicates bacterial taxa enriched in mice treated with antibiotics for 2 days (Q2).

(E) Linear discriminant analysis (LDA) scores of bacterial genera enriched in untreated mice shown in red as negative values; in treated mice for 2 days shown in green as positive values.

(F) Taxonomic cladogram comparing fecal bacterial composition in untreated (red) and treated animals for 4 days (green).

(G) LDA scores of bacterial genera enriched in untreated mice (Q0) shown in red as negative values; in treated mice for 4 days (Q4) shown in green as positive values.

Data represent mean ± SD, n = 8 mice per group. p values are shown as *$p < 0.05$, **$p < 0.01$, ****$p < 0.0001$.

(Khosravi et al., 2014). Of note, the frequency and absolute numbers of Ly6C^{high} cells were not significantly altered in antibiotic-treated versus untreated germ-free (GF) mice (Figure S2) suggesting that perturbation of the monocyte homeostasis is microbiome-mediated rather than a direct toxic effect of the antibiotic cocktail on immune cells. To test whether the antibiotic treatment induced increased cell death of splenic monocytes, we performed an apoptosis assay on Ly6C^{high} monocytes *ex vivo* because apoptotic cells do not accumulate at steady state *in vivo* (Poon et al., 2014). Following antibiotic administration for 3 days, the apoptotic rate was significantly higher in the splenic Ly6C^{high} monocytes from the antibiotic-treated group compared with the control group (Figure 2E). Cell death was not related to bacterial translocation into peripheral organs because we did not detect bacterial growth in mesenteric lymph node, liver, and splenic cell suspensions of mice treated with antibiotics under aerobic and anaerobic conditions (data not shown). Splenic monocytes from antibiotic-treated mice neither underwent increased differentiation to dendritic cells/macrophages nor received signals promoting their immediate exit from the tissue during treatment, as previously shown in angiotensin II-infused mice (Swirski et al., 2009), using an intrasplenic monocyte transfer approach (Figure S3). Taken together, our data demonstrate that decreased levels of PRR ligands in the circulation of antibiotic-treated mice correlate with perturbation of the splenic monocyte homeostasis due to an increased rate of apoptosis in this cell population.

Phenotypic and functional changes in splenic Ly6C^{high} monocytes after depletion of the gut microbiota

Next, we examined the phenotype of splenic monocytes after a 3-day treatment with antibiotics using the Nanostring nCounter platform. RNA profiling of Ly6C^{high} monocytes revealed that genes involved in antigen presentation (*Ciita*, *H2-Aa*, *H2-Ab1*, *Cd74*, *Cd40*, *H2-DMa*) as well as *SOCS3*, *Stat1*, *Traf1*, and *Nkb2* were significantly downregulated following antibiotic treatment (Figure 3A). Significant upregulation was detected for *Trem1*, a triggering receptor; *Cd36*, a phagocytic receptor; *Camp*, cathelicidin anti-microbial peptide (del Fresno et al., 2009); and *S100a8* and *S100a9*, endogenous alarmins that can induce hyporesponsiveness (Austermann et al., 2014). Gene Enrichment Analysis predicted the top 10 biological pathways associated with the differentially expressed (DE) genes such as antigen presentation, interferon and amphoterin signaling, as well as the top 10 putative transcriptional factors regulating their expression (Figure 3B). Changes in expression of *Trem1*, *CD36*, *S100a8*, *S100a9*, *Camp*, and *Ciita* were validated by qPCR (Figure 3C) and were not detected in Ly6C^{high} monocytes from antibiotic-treated GF mice (Figure S2). The aforementioned data suggest that splenic Ly6C^{high} monocytes acquire an immature phenotype marked by decreased expression of antigen-presenting molecules and increased expression of genes involved in phagocytosis and anti-microbial defense at the RNA level following antibiotic treatment.

At the functional level, splenic Ly6C^{high} monocytes from antibiotic-treated mice produced significantly lower levels of TNF-α, IL-6, IL-1α, IL-1β, and IL-10 after lipopolysaccharide (LPS) stimulation compared with control monocytes both at the RNA and protein levels (Figures 3D and 3E). This difference was not due to impaired *ex vivo* survival of splenic monocytes from antibiotic-treated mice, as previously reported (Hergott et al., 2016) (Figure S4). Also, increased phagocytic ability was detected in Ly6C^{high} monocytes from antibiotic-treated mice compared with control mice after intrasplenic injection of fluorescently

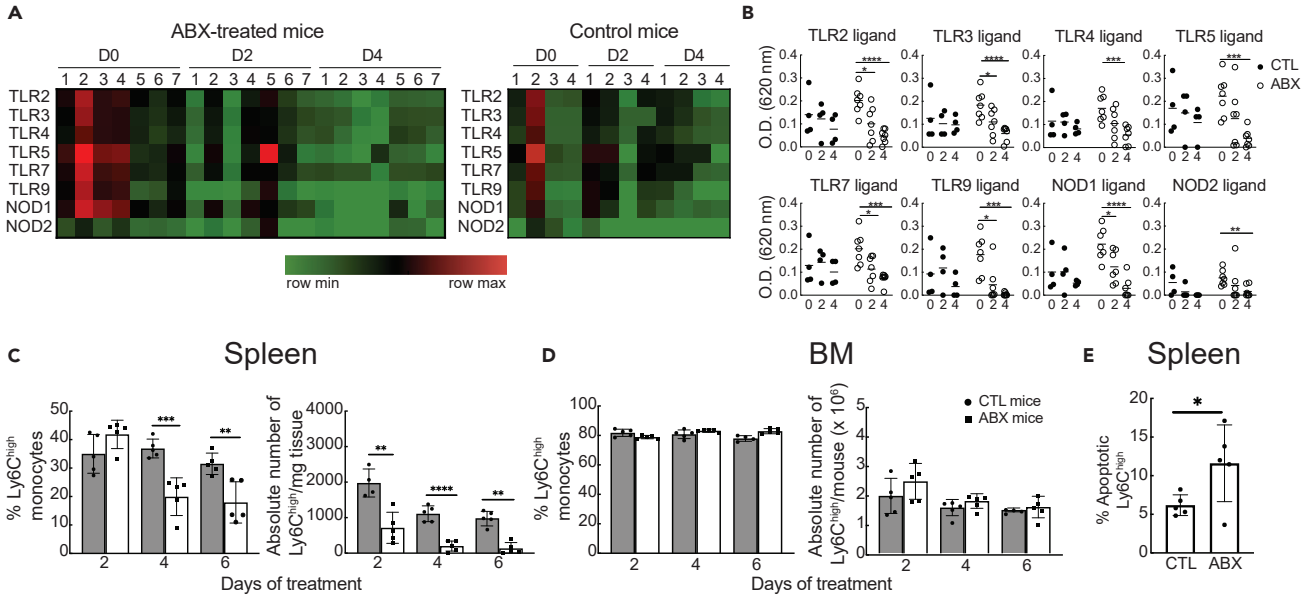

Figure 2. Decreased levels of PRR ligands in the circulation and perturbation of the splenic monocyte homeostasis upon dysbiosis of the gut flora

(A and B) Levels of PRR ligands in the d0, d2, and d4 sera of individual mice treated with (n = 7) or without (n = 4) antibiotics using reporter HEK Blue cells lines for detection as described in transparent methods. In the heatmap, each column represents the serum response of an individual mouse against the PRR ligand listed in each row. Each cell line was incubated with serum in duplicate wells. Data are representative of four independent experiments. Statistical significance was assessed by paired Student's t test.

(C and D) Frequency and absolute number of Ly6C^{high} monocytes in the (C) spleen and (D) BM of mice treated with or without antibiotics for the indicated time period. Flow cytometric analysis was gated on live LIN^{-}CD11b^{+} cells as described in transparent methods. Absolute number of Ly6C^{high} monocytes was normalized to milligrams of tissue for spleen, whereas total BM cells recovered from each mouse are shown for BM. Data show the mean ± SEM, and they are representative of three independent experiments (n = 6 per group).

(E) *Ex vivo* detection of apoptosis in splenic Ly6C^{high} monocytes from mice treated with or without antibiotics for 3 days. Splenocyte suspensions were incubated with FAM-FLIVO, and 1 h later, cells were washed twice and fixed and analyzed by flow cytometry.

Data show the frequency of apoptotic cells gated on Ly6C^{high} monocytes (mean ± SEM, n = 5 mice per group). Statistical significance was assessed by Student's t test. p values are shown as *p < 0.05, **p < 0.01, ***p < 0.001, ****p < 0.0001.

labeled microspheres (Figure 3F). Finally, Ly6C^{high} monocytes had a higher anti-microbial capacity toward *E. coli*, K12 strain, and *Citrobacter rodentium* compared with the control group in a gentamicin protection assay (Figure 3G). Overall, these results demonstrate that splenic Ly6C^{high} monocytes acquire an immature phenotype with decreased expression of antigen-presenting molecules accompanied by decreased production of inflammatory cytokines and increased phagocytic and anti-microbial abilities following gut dysbiosis.

Addition of PRR ligands restores splenic Ly6C^{high} monocyte numbers and functions in antibiotic-treated mice

Last, we investigated whether addition of certain PRR ligands in the circulation would restore splenic monocyte homeostasis and function in antibiotic-treated mice. As described in transparent methods, after a 3-day treatment with antibiotics, mice were injected intraperitoneally (i.p.) with low levels of (1) a TLR ligand (TLRL) cocktail, (2) ie-DAP (a NOD1 ligand), or (3) MDP (a NOD2 ligand). Injection of ie-DAP, but not of TLRL cocktail or MDP, in antibiotic-treated mice increased the frequency and the absolute numbers of splenic Ly6C^{high} cells (Figure 4A). At the functional level, the phagocytic ability of splenic Ly6C^{high} cells from antibiotic-treated mice was restored to levels similar to the untreated group when mice were injected with the TLRL cocktail but not with ie-DAP or MDP (Figure 4B). In terms of cytokines, we monitored the production of TNF-α and IL-6 in *ex vivo*-obtained Ly6C^{high} monocytes after LPS stimulation. In antibiotic-treated mice, ie-DAP and MDP, but not TLRL cocktail, produced TNF-α at similar or higher levels compared with untreated mice (Figure 4C). Interestingly, injection of any of the PRR ligands restored the synthesis of IL-6 in cells from the treated group (Figure 4C). Regarding the antimicrobial capacity of splenic Ly6C^{high} monocytes, addition of TLRL cocktail and MDP in antibiotic-treated mice brought back to control levels the ability of *C. rodentium* and *E. coli* to survive intracellularly (Figure 4D). Taken together, our data suggest that

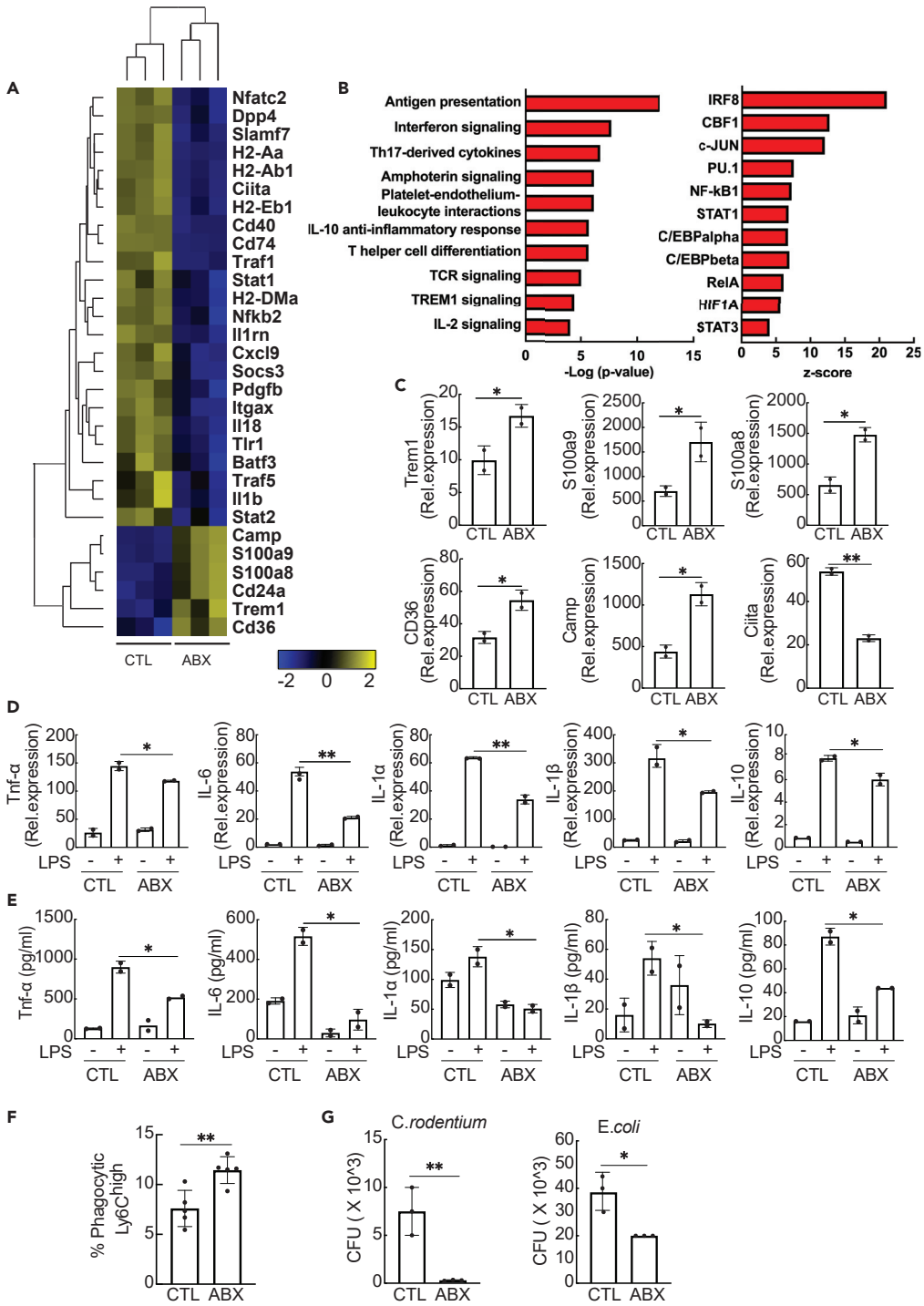

Figure 3. Phenotypic and functional changes in splenic Ly6C^{high} monocytes after depletion of the gut microbiota

(A) Heatmap depicting hierarchical clustering of significantly upregulated (yellow) and downregulated (blue) genes in splenic Ly6C^{high} monocytes from untreated and treated animals for 3 days as calculated by the nSolver software.

(B) The 10 most significant biological networks and 10 top upstream transcriptional regulators of the DE genes of Ly6C^{high} monocytes as predicted by the MetaCore software.

(C) Validation of changes in gene expression of *Trem-1*, *S100a8*, *S100a9*, *Cd36*, *Camp*, and *Ciita* by qPCR. Gene expression is presented relative to *Gapdh*. Data show mean ± SEM, and they are representative of two experiments (n = 10 for antibiotic-treated group, n = 5 for control group).

Figure 3. *Continued*

(D) Quantitative PCR analysis of the expression of *Tnf-α*, *IL-6*, *IL-1α*, *IL-1β*, and *IL-10* in splenic Ly6C^{high} monocytes from antibiotic-treated and untreated mice after *ex vivo* stimulation with or without LPS. Gene expression has been normalized to *Gapdh*. Data show mean ± SD, and they are representative of two experiments (n = 10 for antibiotic-treated group, n = 5 for control group).

(E) Detection of Tnf-α, IL-6, IL-1α, IL-1β, and IL-10 in the culture supernatant of splenic Ly6C^{high} monocytes from antibiotic-treated and untreated mice after *ex vivo* stimulation with or without LPS. Data show mean ± SD, and they are representative of two experiments (n = 10 for antibiotic-treated group, n = 5 for control group).

(F) Percentage of splenic Ly6C^{high} monocytes from antibiotic-treated and untreated mice containing fluorescently labeled beads, 24 h after intra-splenic bead injection (n = 7 per group). Data show mean ± SD, and they are representative of two experiments.

(G) Gentamicin protection assay on splenic Ly6C^{high} monocytes from antibiotic-treated and untreated mice with *C. rodentium* and *E. coli*. Values (mean ± SD) show absolute colony-forming unit (CFU) counts after overnight incubation of cell lysates at 37°C and are representative of three experiments (n = 10 for antibiotic-treated group, n = 5 for control group).

Statistical significance was assessed by Student's t test for pairwise comparisons. p values are shown as *$p < 0.05$, **$p < 0.01$.

addition of certain PRR ligands in the circulation of antibiotic-treated mice restores the numbers and normal function of splenic Ly6C^{high} monocytes. These findings highlight that (1) perturbation of the splenic Ly6C^{high} numbers and function in antibiotic-treated mice is caused by the absence of certain circulating PRR ligands and (2) circulating PRR ligands have diverse and pleiotropic effects on the immune functions of splenic Ly6C^{high} monocytes.

DISCUSSION

In this study, we examined whether circulating PRR ligands produced constitutively by the gut microbiome regulate the splenic Ly6C^{high} monocyte homeostasis and function during steady state. Our study focused on splenic Ly6C^{high} monocytes as these immune cells play a regulatory role in the pathogenesis of many diseases such as EAE (Zhu et al., 2007; Melero-Jerez et al., 2020), ALS (Butovsky et al., 2012), stroke (Seifert and Offner, 2018; Pennypacker and Offner, 2015), atherosclerosis (Robbins et al., 2012; Swirski et al., 2016), ischemic myocardial injury (Leuschner et al., 2012; Swirski et al., 2009), lung ischemia-reperfusion injury (Hsiao et al., 2018), colitis (Griseri et al., 2012) and several tumor models (Cortez-Retamozo et al., 2012; Richards et al., 2013; Wu et al., 2018). We induced dysbiosis of the gut microbiome by administering a broad-spectrum antibiotic cocktail for a very short time period, compared with other studies (Kennedy et al., 2018), to identify the *direct* role of circulating PRR ligands on the maintenance of monocytes. Our findings delineate a new level of regulation by the microbiome in addition to the regulation of hematopoiesis, previously described in experiments with a 2- to 5-week exposure to antibiotics (Josefsdottir et al., 2017; Khosravi et al., 2014). Similar observations have been reported for neutrophils where the gut microbiome directly affects their function in blood in addition to their production in the BM (Zhang and Frenette, 2019). We conducted our experiments using female mice as the innate immune responses are generally stronger in females than in males (Klein and Flanagan, 2016) and the intestinal microbiota appears consistent throughout the estrous cycle (Wallace et al., 2018).

In our study, we identified the S24_7 and Rikenellaceae families (Bacteroidetes phylum); Clostridiaceae, Lachnospiraceae, Ruminococcaceae, and Mogibacteriaceae families (Firmicutes phylum); Mollicutes RF39 (Tenericutes phylum); and Bifidobacterium (Actinobacteria phylum) as the most susceptible taxa to our antibiotic treatment. This finding, in combination with the parallel reduction of PRR ligands in the circulation of treated animals, demonstrates that these bacterial families may be among the primary sources of PRR ligand production within the gut during steady state. Conversely, our data suggest that all the bacterial taxa that underwent significant expansion during the treatment, including *Sutterella*, *Staphylococcus*, and *Akkermansia muciniphila*, may not contribute significantly to the production of circulating PRR ligands. The simultaneous perturbation of the gut microbiota homeostasis and reduction of PRR ligands from the circulation of antibiotic-treated animals further supports the premise that the gut microbiome constitutively produces and secretes bacterial-derived products in the circulation, as previously shown in antibiotic, streptozotoxin-treated mice (Thaiss et al., 2018). To our knowledge, our data report for the first time the simultaneous presence of TLR2, 3, 4, 5, 7, and 9 and NOD1 and NOD2 ligands at low levels in the sera of naive animals, supporting previous studies that have detected NOD1 (Clarke et al., 2010), NOD2 (Huang et al., 2019) and TLR2 (Farrokhi et al., 2013) ligands in the circulation of naive mice.

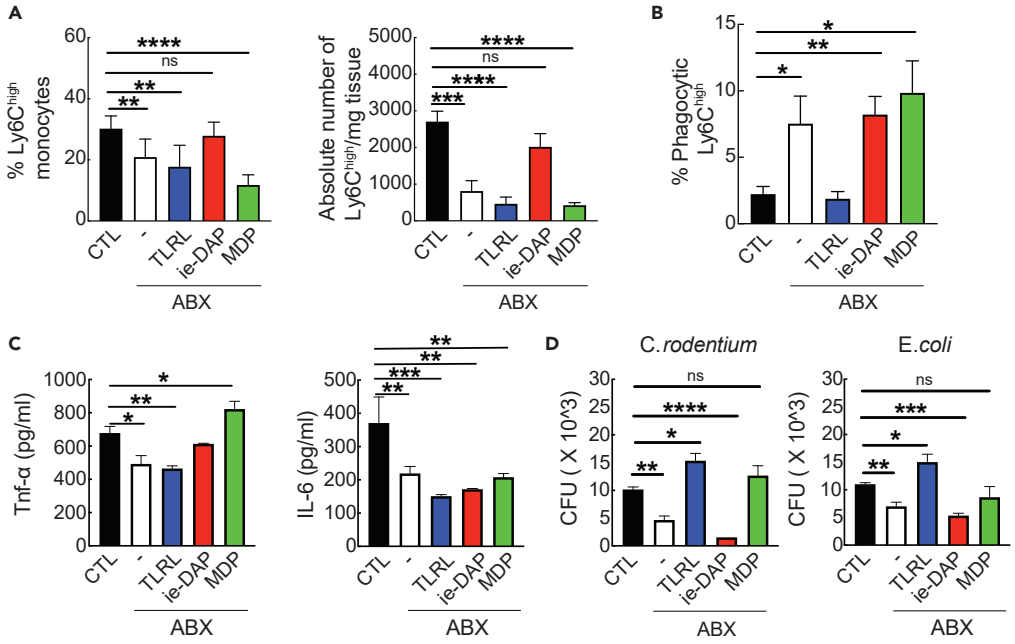

Figure 4. Addition of PRR ligands restores splenic Ly6C^{high} monocyte number and functions in antibiotic-treated mice

(A) Percentage and absolute number of splenic Ly6C^{high} monocytes from untreated and antibiotic-treated mice injected i.p. with either ie-DAP, MDP, or TLRL or PBS. Data show mean ± SD and are representative of two experiments (n = 6 per group).

(B) Percentage of splenic Ly6C^{high} monocytes from untreated and antibiotic-treated mice injected i.p. with either ie-DAP, MDP, or TLRL or PBS containing fluorescently labeled beads. Flow cytometric analysis was assessed 24 h after intra-splenic bead injection (n = 6 per group). Data show mean ± SD, and they are representative of three experiments.

(C) Presence of TNF-α and IL-6 in the culture supernatant of LPS-stimulated splenic Ly6C^{high} monocytes from untreated and antibiotic-treated mice injected i.p. with either ie-DAP, MDP, or TLRL or PBS. Data (mean ± SD) are representative of two experiments (n = 6 per group).

(D) Gentamicin protection assay on splenic Ly6C^{high} monocytes from untreated and antibiotic-treated mice injected i.p. with either ie-DAP, MDP, or TLRL or PBS with *C. rodentium* and *E. coli*. Absolute CFU counts (mean ± SD) after overnight incubation of cell lysates at 37°C are representative of two experiments (n = 6 per group).

Statistical significance was assessed by one-way ANOVA test for pairwise comparisons. p values are shown as *p < 0.05, **p < 0.01, ***p < 0.001, ****p < 0.0001.

Reduction of PRR ligands from the circulation of antibiotic-treated mice was associated with perturbation of splenic but not BM-derived Ly6C^{high} monocytes. This observation could be explained either by a differential regulation of spleen versus BM-derived monocytes by the gut microbiome or by a prompt replenishment of monocytes by progenitors within the BM of treated animals. Our data propose that the homeostasis of splenic Ly6C^{high} monocytes does not depend alone on BM hematopoiesis effects as suggested earlier (Khosravi et al., 2014) but that it can also be impacted directly by signals from commensal bacteria. This apparent discrepancy could be due to the short-term antibiotic treatment we performed (4 days) versus the long-term treatment (4–5 weeks) performed by Khosravi *et al.* Disruption of the monocyte homeostasis is microbiome-mediated because we did not observe similar changes in the numbers of splenic Ly6C^{high} monocytes in antibiotic-treated GF animals. Perturbation was also related to increased apoptotic rate within the spleen further supporting that deprivation of gut microbiota-derived signals has an immediate impact on the homeostasis of splenic monocytes. We did not detect increased differentiation to DC/macrophages or increased trafficking of monocytes from the spleen to the bloodstream or to the gut of antibiotic-treated mice in response to increased bacterial cell death.

Splenic Ly6C^{high} monocytes underwent transcriptional and functional changes after 3 days of antibiotic administration. Molecules involved in antigen presentation pathways (*Ciita*, *H2-Aa*, *H2-Ab1*, *Cd74*, *Cd40*, *H2-DMa*) as well as *Stat1*, *Traf1*, and *Nkb2* were significantly downregulated, whereas *Trem1*, a

proinflammatory factor; *CD36*, a scavenger receptor; and *Camp*, an antimicrobial peptide, were significantly upregulated. Functionally, Ly6C^{high} monocytes from antibiotic-treated mice produced lower levels of proinflammatory cytokines and they had acquired increased phagocytic and antimicrobial abilities, hallmarks of endotoxin-tolerant monocytes (del Fresno et al., 2009). It could be that in the absence of circulating tonic signals, S100a8 and S100a9, two calcium-binding proteins, act as endogenous alarmins inducing a state of hyporesponsiveness to monocytes, similar to exogenous LPS (Austermann et al., 2014).

As dysbiosis of the gut microbiome can destabilize the whole metabolome signature in the circulation (Vernocchi et al., 2016), we addressed whether perturbation of the splenic Ly6C^{high} monocyte numbers and function in antibiotic-treated mice is specifically regulated by the levels of circulating PRR ligands. We report that the NOD1 signaling pathway regulates the lifespan of splenic Ly6C^{high} monocytes confirming findings from a previous study (Hergott et al., 2016). The presence of TLRL increased the phagocytic properties of Ly6C^{high} cells, as has previously been described in cell lines *in vitro* (Doyle et al., 2004). Further studies need to address which TLRL, individually or in combination, has this regulatory role. Interestingly, our observation that the antimicrobial capacity of Ly6C^{high} monocytes is regulated by TLRL and MDP is in agreement with previous studies suggesting enhancement of the antimicrobial capacity of phagocytes by TLRs (Brightbill et al., 1999) and MDP (O'Reilly and Zak, 1992). In terms of cytokine production, the levels of TNF-α were restored after injection of ie-DAP and MDP in LPS-stimulated Ly6C^{high} monocytes, whereas any PRR ligand affected the production of IL-6. Our data demonstrate that individual circulating PRR ligands have pleiotropic effects on the immune functions of splenic Ly6C^{high} monocytes. Further studies will be performed to dissect the underlying mechanisms of these complex interactions. Also, in our study, we have not addressed the impact of the gut dysbiosis on the levels of other microbial metabolites, such as SCFAs, β-glucans, and bile acids, known to affect the biology of monocytes (Fiorucci et al., 2018; van de Wouw et al., 2019).

Taken together, our findings suggest that the ecology of the intestinal microbiota can control the homeostasis and function of splenic Ly6C^{high} monocytes during steady state via regulation of the levels of circulating PRR ligands. Identification of the PRR ligand-monocyte crosstalk provides an opportunity to develop intervention strategies to modulate splenic monocytes, an important immune cell subset in the pathogenesis of cardiovascular and CNS-related diseases.

Limitations of the study

In this study we demonstrate that circulating PRR ligands produced by the gut microbiome regulate the number and immune functions of splenic Ly6C^{high} monocytes. Whether circulating PRR ligands act directly upon splenic Ly6C^{high} monocytes or indirectly via other immune cells *in vivo* can be further investigated in future studies.

Resource availability

Lead contact

Howard L. Weiner, Ann Romney Center for Neurologic Diseases, Brigham and Women's Hospital, Harvard Medical School, Building for Transformative Medicine, 60 Fenwood Road, 10002G, Boston, MA, 02115-6128, hweiner@rics.bwh.harvard.edu.

Materials availability

This study did not generate new unique reagents.

Data and code availability

The raw data from the 16S rRNA sequencing library and the Nanostring data have been uploaded in Mendeley (https://doi.org/10.17632/tjdwjnzskr.1).

All datasets supporting the current study are available from the corresponding author on request.

METHODS

All methods can be found in the accompanying Transparent Methods supplemental file.

SUPPLEMENTAL INFORMATION

Supplemental information can be found online at https://doi.org/10.1016/j.isci.2021.102356.

ACKNOWLEDGMENTS

We thank Vladimir Yeliseyev for technical assistance with GF mouse experiments, Joseph Rone for technical assistance with bacterial cultures, Kit Fuhrman and Clement David for assistance with analysis of Nanostring data, Biopolymers Facility at Harvard Medical School for sequencing data, and Deneen E. Kozoriz and Rajesh K. Krishnan for sorting. The research was supported by NIH grant RO1# NS087226 to H.W.

AUTHOR CONTRIBUTIONS

Conceptualization, P.K. and H.L.W.; investigation, P.K., A.S., and V.W.; methodology, P.K., S.L., L.M.C., M.F., R.R., and D.G.; resources: S.L.; formal analysis, P.K., L.M.C., and V.W.; writing – original draft, P.K. and H.L.W.; writing – review & editing, P.K. and H.L.W.; funding acquisition, H.L.W.; supervision, H.L.W.

DECLARATION OF INTERESTS

The authors declare no competing interests.

Received: December 30, 2020
Revised: February 17, 2021
Accepted: March 22, 2021
Published: April 23, 2021

REFERENCES

Anstadt, E.J., Fujiwara, M., Wasko, N., Nichols, F., and Clark, R.B. (2016). TLR tolerance as a treatment for central nervous system. Autoimmun. J. Immunol. *197*, 2110–2118.

Austermann, J., Friesenhagen, J., Fassl, S.K., Petersen, B., Ortkras, T., Burgmann, J., Barczyk-Kahlert, K., Faist, E., Zedler, S., Pirr, S., et al. (2014). Alarmins MRP8 and MRP14 induce stress tolerance in phagocytes under sterile inflammatory conditions. Cell Rep. *9*, 2112–2123.

Balmer, M.L., Schürch, C.M., Saito, Y., Geuking, M.B., Cuenca, M., Kovtonyuk, L.V., McCoy, K.D., Hapfelmeier, S., and Ochsenbein, A.F. (2014). Microbiota-derived compounds drive steady-state granulopoiesis via MyD88/TICAM signaling. J. Immunol. *193*, 5273–5283.

Belkaid, Y., and Harrison, O.J. (2017). Homeostatic immunity and the microbiota. Immunity *46*, 562–576.

Blomster, L.V., Brennan, F.H., Lao, H.W., Harle, D.W., Harvey, A.R., and Ruitenberg, M.J. (2013). Mobilisation of the splenic monocyte reservoir and peripheral CX$_3$CR1 deficiency adversely affects recovery from spinal cord injury. Exp. Neurol. *247*, 226–240.

Brightbill, H.D., Libraty, D.H., Krutzik, S.R., Yang, R.B., Belisle, J.T., Bleharski, J.R., Maitland, M., Norgard, M.V., Plevy, S.E., Smale, S.T., et al. (1999). Host defense mechanisms triggered by microbial lipoproteins through toll-like receptors. Science *285*, 732–736.

Butovsky, O., Siddiqui, S., Gabriely, G., Lanser, A.J., Ben, Dake, Murugaiyan, G., Doykan, C.E., Wu, P.M., Gali, R.R., Iyer, L.K., et al. (2012). Modulating inflammatory monocytes with a unique microRNA gene signature ameliorates murine ALS. J. Clin. Invest. *122*, 3063–3087.

Clarke, T.B., Davis, K.M., Lysenko, E.S., Zhou, A.Y., Yu, Y., and Weiser, J.N. (2010). Recognition of peptidoglycan from the microbiota by Nod1 enhances systemic innate immunity. Nat. Med. *16*, 228–231.

Cortez-Retamozo, V., Etzrodt, M., Newton, A., Rauch, P.J., Chudnovskiy, A., Berger, C., Ryan, R.J.H., Iwamoto, Y., Marinelli, B., Gorbatov, R., et al. (2012). Origins of tumor-associated macrophages and neutrophils. Proc. Natl. Acad. Sci. U S A *109*, 2491–2496.

del Fresno, C., Garcia-Rio, F., Gomez-Pina, V., Soares-Schanoski, A., Fernandez-Ruiz, I., Jurado, T., Kajiji, T., Shu, C., Marin, E., Gutierrez del Arroyo, A., et al. (2009). Potent phagocytic activity with impaired antigen presentation identifying lipopolysaccharide-tolerant human monocytes: demonstration in isolated monocytes from cystic fibrosis patients. J. Immunol. *183*, 2194.

Doyle, S.E., O'Connell, R.M., Miranda, G.A., Vaidya, S.A., Chow, E.K., Liu, P.T., Suzuki, S., Suzuki, N., Modlin, R.L., Yeh, W.-C., et al. (2004). Toll-like receptors induce a phagocytic gene program through p38. J. Exp. Med. *199*, 81–90.

Farrokhi, V., Nemati, R., Nichols, F.C., Yao, X., Anstadt, E., Fujiwara, M., Grady, J., Wakefield, D., Castro, W., Donaldson, J., et al. (2013). Bacterial lipodipeptide, Lipid 654, is a microbiome-associated biomarker for multiple sclerosis. Clin. Transl. Immunol. *2*, e8.

Fiorucci, S., Biagioli, M., Zampella, A., and Distrutti, E. (2018). Bile acids Activated receptors regulate innate immunity. Front. Immunol. *9*, 1853.

Giladi, A., Wagner, L.K., Li, H., Dörr, D., Medaglia, C., Paul, F., Shemer, A., Jung, S., Yona, S., Mack, M., et al. (2020). Cxcl10+ monocytes define a pathogenic subset in the central nervous system during autoimmune neuroinflammation. Nat. Immunol. *21*, 525–534.

Gorjifard, S., and Goldszmid, R.S. (2016). Microbiota–myeloid cell crosstalk beyond the gut. J. Leukoc. Biol. *100*, 865–879.

Griseri, T., McKenzie, B.S., Schiering, C., and Powrie, F. (2012). Dysregulated hematopoietic stem and progenitor cell activity promotes interleukin-23-driven chronic intestinal inflammation. Immunity *37*, 1116–1129.

Guilliams, M., Mildner, A., and Yona, S. (2018). Developmental and functional heterogeneity of monocytes. Immunity *49*, 595–613.

Hergott, C.B., Roche, A.M., Tamashiro, E., Clarke, T.B., Bailey, A.G., Laughlin, A., Bushman, F.D., and Weiser, J.N. (2016). Peptidoglycan from the gut microbiota governs the lifespan of circulating phagocytes at homeostasis. Blood *127*, 2460–2471.

Hsiao, H.-M., Fernandez, R., Tanaka, S., Li, W., Spahn, J.H., Chiu, S., Akbarpour, M., Ruiz-Perez, D., Wu, Q., Turam, C., et al. (2018). Spleen-derived classical monocytes mediate lung ischemia-reperfusion injury through IL-1β. J. Clin. Invest. *128*, 2833–2847.

Huang, Z., Wang, J., Xu, X., Wang, H., Qiao, Y., Chu, W.C., Xu, S., Chai, L., Cottier, F., Pavelka, N., et al. (2019). Antibody neutralization of microbiota-derived circulating peptidoglycan dampens inflammation and ameliorates autoimmunity. Nat. Microbiol. *4*, 766–773.

Josefsdottir, K.S., Baldridge, M.T., Kadmon, C.S., and King, K.Y. (2017). Antibiotics impair murine hematopoiesis by depleting the intestinal microbiota. Blood *129*, 729–739.

Kennedy, E.A., King, K.Y., and Baldridge, M.T. (2018). Mouse microbiota models: comparing germ-free mice and antibiotics treatment as tools for modifying gut bacteria. Front. Physiol. *9*, 1534.

Khosravi, A., Yáñez, A., Price, J.G., Chow, A., Merad, M., Goodridge, H.S., and Mazmanian, S.K. (2014). Gut microbiota promote hematopoiesis to control bacterial infection. Cell Host Microbe *15*, 374–381.

Kim, C.H. (2018). Immune regulation by microbiome metabolites. Immunology *154*, 220–229.

Klein, S.L., and Flanagan, K.L. (2016). Sex differences in immune responses. Nat. Rev. Immunol. *16*, 626–638.

Leuschner, F., Rauch, P.J., Ueno, T., Gorbatov, R., Marinelli, B., Lee, W.W., Dutta, P., Wei, Y., Robbins, C., Iwamoto, Y., et al. (2012). Rapid monocyte kinetics in acute myocardial infarction are sustained by extramedullary monocytopoiesis. J. Exp. Med. *209*, 123–137.

Melero-Jerez, C., Alonso-Gómez, A., Moñivas, E., Lebrón-Galán, R., Machín-Díaz, I., de Castro, F., and Clemente, D. (2020). The proportion of myeloid-derived suppressor cells in the spleen is related to the severity of the clinical course and tissue damage extent in a murine model of multiple sclerosis. Neurobiol. Dis. *140*, 104869.

O'Reilly, T., and Zak, O. (1992). Enhancement of the effectiveness of antimicrobial therapy by muramyl peptide immunomodulators. Clin. Infect. Dis. *14*, 1100–1109.

Pennypacker, K.R., and Offner, H. (2015). The role of the spleen in ischemic stroke. J. Cereb. Blood Flow Metab. *35*, 186–187.

Poon, I.K.H., Lucas, C.D., Rossi, A.G., and Ravichandran, K.S. (2014). Apoptotic cell clearance: basic biology and therapeutic potential. Nat. Rev. Immunol. *14*, 166–180.

Richards, D.M., Hettinger, J., and Feuerer, M. (2013). Monocytes and macrophages in cancer: development and functions. Cancer Microenviron. *6*, 179–191.

Robbins, C.S., Chudnovskiy, A., Raunch, P.J., Figueiredo, J.-L., Iwamoto, Y., Gorbatov, R., Etzrodt, M., Weber, G.F., Ueno, T., and Rooijen, N.V. (2012). Extramedullary hematopoiesis generates Ly-6C(high) monocytes that infiltrate atherosclerotic lesions. Circulation *125*, 364–374.

Seifert, H.A., and Offner, H. (2018). The splenic response to stroke: from rodents to stroke subjects. J. Neuroinflamm. *15*, 195.

Swirski, F.K., Nahrendorf, M., Etzrodt, M., Wildgruber, M., Cortez-Retamozo, V., Panizzi, P., Figueiredo, J.-L., Kohler, R.H., Chudnovskiy, A., Waterman, P., et al. (2009). Identification of splenic reservoir monocytes and their deployment to inflammatory sites. Science *325*, 612–616.

Swirski, F.K., Nahrendorf, M., and Libby, P. (2016). Mechanisms of Myeloid Cell Modulation of Atherosclerosis. Microbiol. Spectr. *4*.

Thaiss, C.A., Levy, M., Grosheva, I., Zheng, D., Soffer, E., Blacher, E., Braverman, S., Tengeler, A.C., Barak, O., Elazar, M., et al. (2018). Hyperglycemia drives intestinal barrier dysfunction and risk for enteric infection. Science *359*, 1376–1383.

van de Wouw, M., Boehme, M., Dinan, T.G., and Cryan, J.F. (2019). Monocyte mobilisation, microbiota & mental illness. Brain Behav. Immun. *81*, 74–91.

Vernocchi, P., Del Chierico, F., and Putignani, L. (2016). Gut microbiota profiling: metabolomics based approach to unravel compounds affecting human health. Front. Microbiol. *7*, 1144.

Wallace, J.G., Potts, R.H., Szamosi, J.C., Surette, M.G., and Sloboda, D.M. (2018). The murine female intestinal microbiota does not shift throughout the estrous cycle. PLoS One *13*, e0200729.

Wu, C., Ning, H., Liu, M., Lin, J., Luo, S., Zhu, W., Xu, J., Wu, W.-C., Liang, J., Shao, C.-K., et al. (2018). Spleen mediates a distinct hematopoietic progenitor response supporting tumor-promoting myelopoiesis. J. Clin. Invest. *128*, 3425–3438.

Zhang, D., and Frenette, P.S. (2019). Cross talk between neutrophils and the microbiota. Blood *133*, 2168–2177.

Zhu, B., Bando, Y., Xiao, S., Yang, K., Anderson, A.C., Kuchroo, V.K., and Khoury, S.J. (2007). CD11b+Ly-6C(hi) suppressive monocytes in experimental autoimmune encephalomyelitis. J. Immunol. *179*, 5228–5237.

iScience, Volume *24*

Supplemental information

Regulation of splenic monocyte homeostasis and function by gut microbial products

Panayota Kolypetri, Shirong Liu, Laura M. Cox, Mai Fujiwara, Radhika Raheja, Dvora Ghitza, Anya Song, Dominique Daatselaar, Valerie Willocq, and Howard L. Weiner

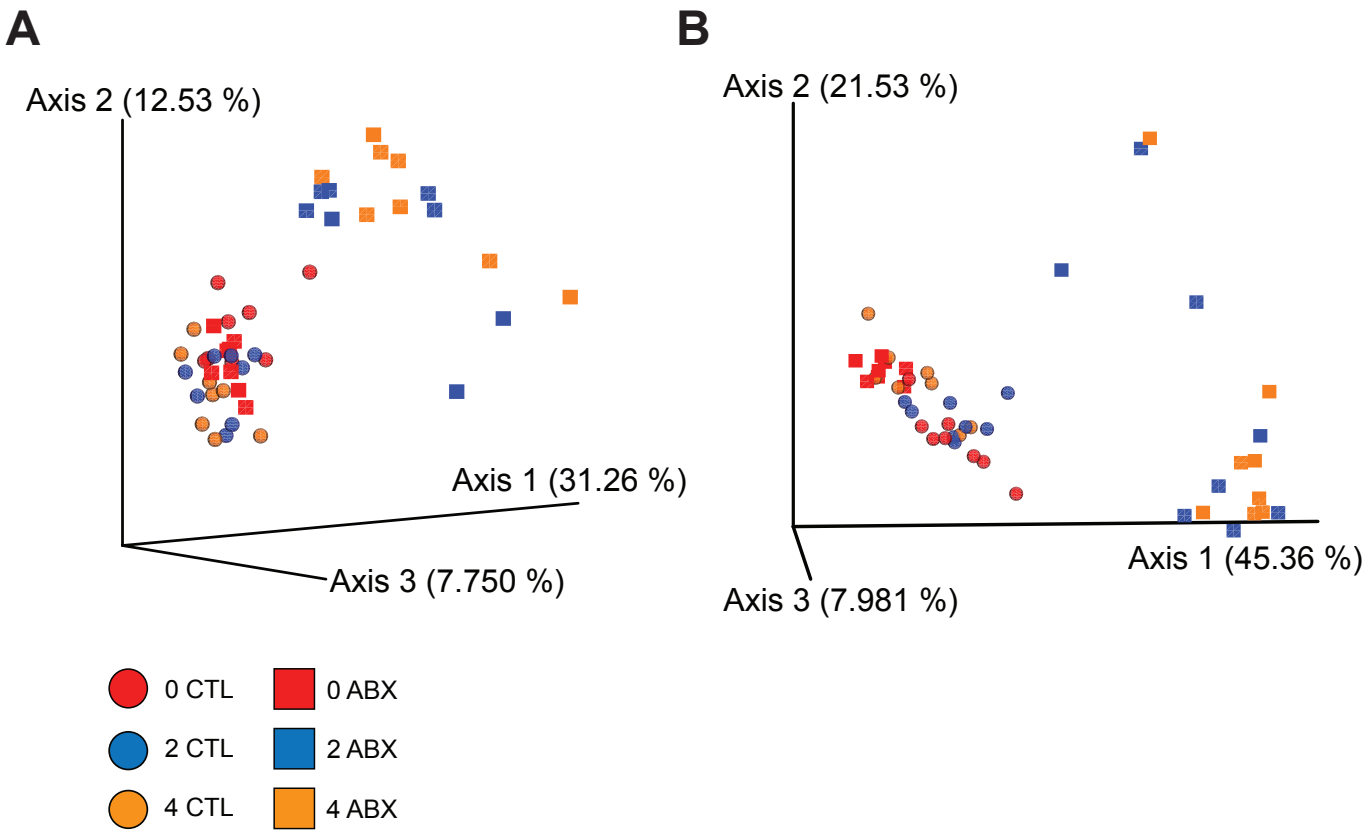

Figure S1. Alterations in the composition of the gut microbiome after a short-term antibiotic treatment. Related to Figure 1.

Principal coordinates analysis (PCoA) of the A) unweighted and B) weighted Unifrac distances of the 16S rRNA sequencing data as visualized by Emperor. The two groups are represented by colored circles (untreated mice) and squares (antibiotic-treated mice). Timepoints are shown in red (day 0), blue (day 2), and orange (day 4) color. Differences between the antibiotic-treated and untreated group were statistical significant as calculated by the permanova paired wise test.

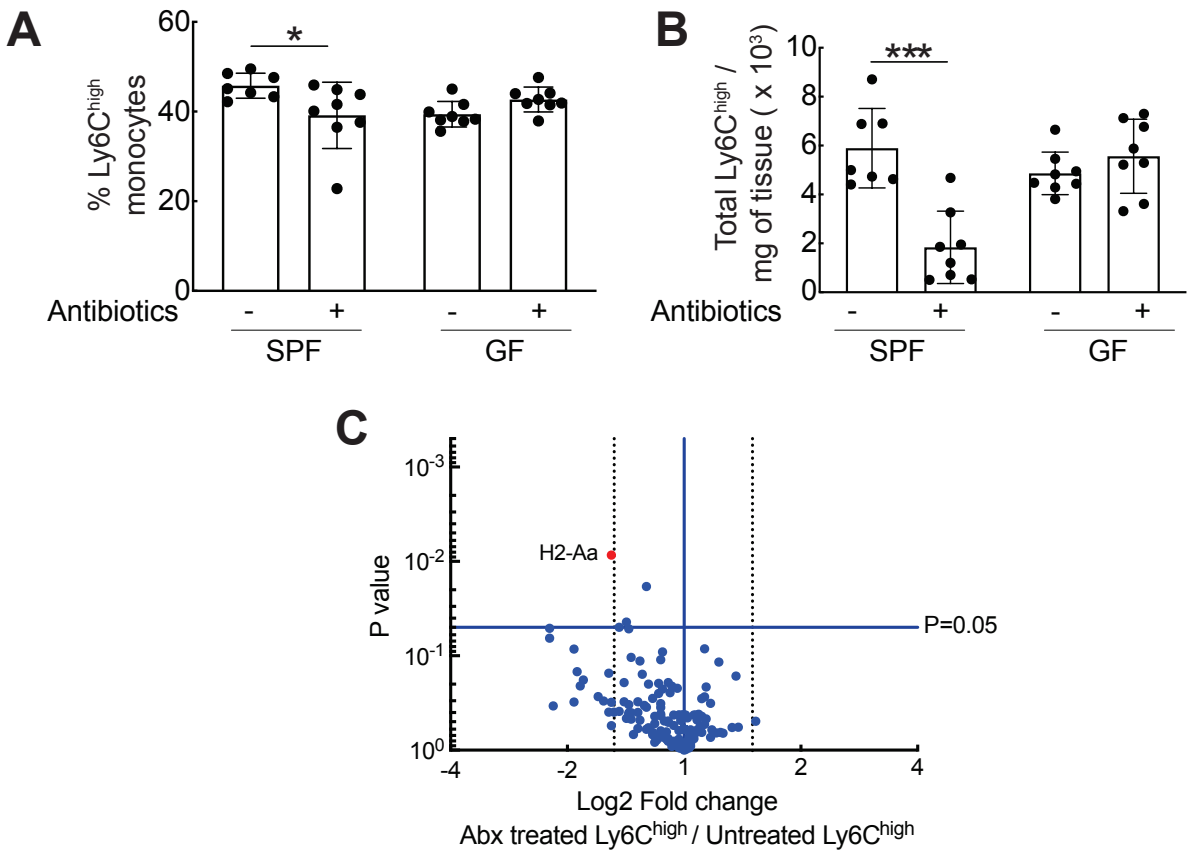

Figure S2. Perturbation of splenic Ly6C^{high} monocyte homeostasis in antibiotic-treated mice is microbiome-mediated. Related to Figure 2 and 3.

SPF and GF mice were treated with or without the antibiotic cocktail for 4 days. On day 4, the frequency and absolute numbers of Ly6C^{high} monocytes were estimated by flow cytometry. A) Frequency and B) absolute number per mg of tissue of splenic Ly6C^{high} monocytes from antibiotic-treated and untreated SPF and GF mice. Data show the mean ± s.dev. (n=7-8 mice per group). Statistical significance was assessed by two-tailed student's t test. * $p < 0.05$, ** $p < 0.01$, *** $p < 0.001$; C) Volcano plot showing fold changes in gene expression in splenic Ly6C^{high} monocytes from antibiotic-treated vs untreated GF mice using the nCounter Nanostring Immunology panel. Each dot presents one gene while the color of the dot shows the significance in the change of gene expression. A fold change ≥ 1.5 (upregulation) and ≤ -1.5 (downregulation) was considered significant whereas p values were calculated by the nSolver analysis software. Blue dots represent genes with no statistically significant change in their expression whereas red dots show genes which expression levels were significantly affected by the antibiotic treatment.

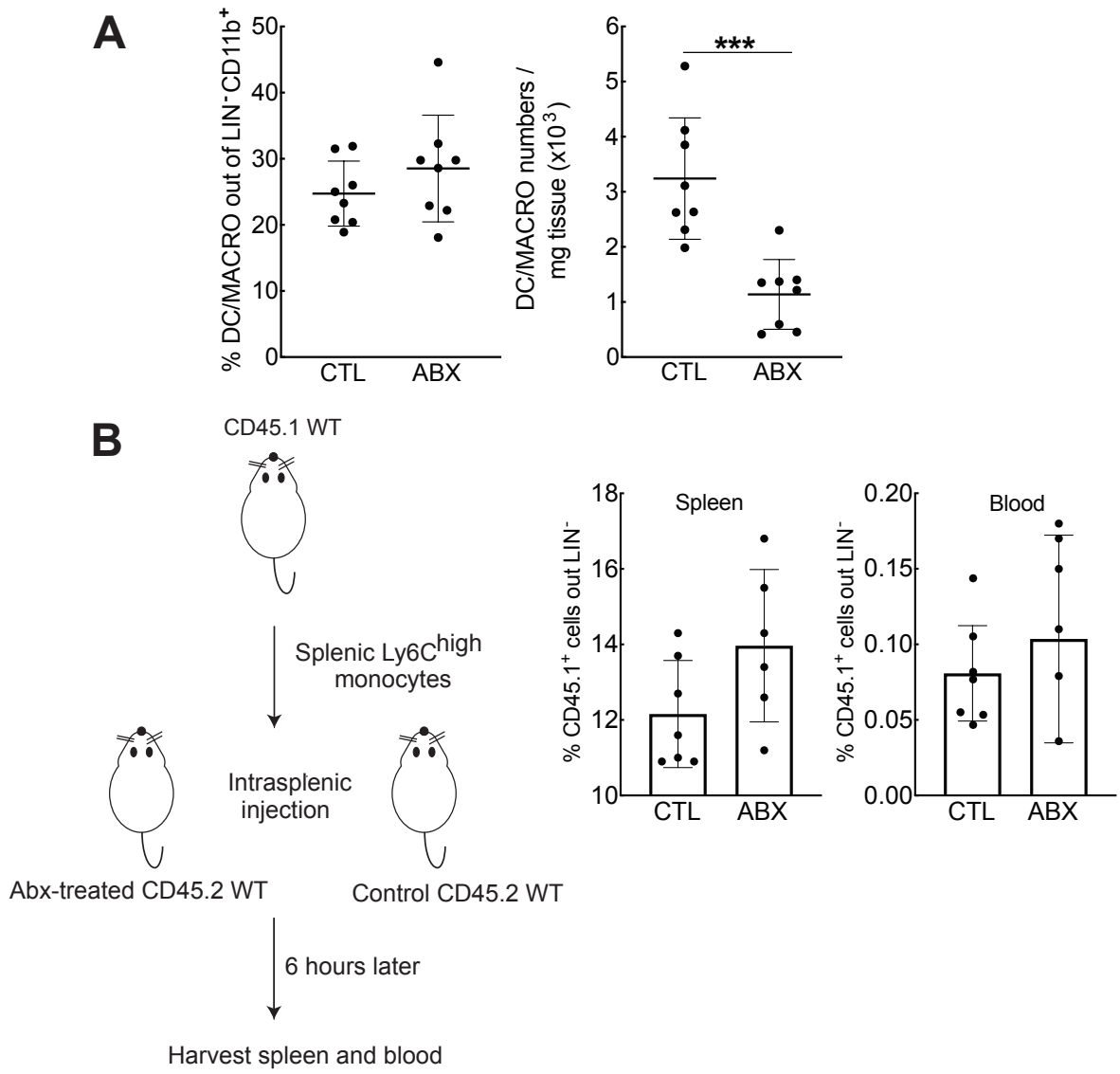

Figure S3. Perturbation of the splenic Ly6C^{high} monocyte homeostasis after gut dysbiosis is not related to increased differentiation to DC/macrophages or increased exit from the tissue. Related to Figure 2.

A) Frequency and absolute number of DC/macrophages in splenic cell suspensions of mice treated with or without antibiotics for 3 days. Data show mean ± s.dev. and they are representative of two experiments (n=6 per group). Statistical significance was assessed by Student's t-test. P values are shown as *p<0.05, **p<0.01, ***p<0.001; B) Experimental design of intrasplenic transfer of CD45.1^{+} splenic Ly6C^{high} monocytes to CD45.2^{+} C57BL/6 mice, pretreated with or without antibiotics for 3 days. Data show frequency of CD45.1^{+} cells out of LIN- in splenic cell suspensions and blood six hours after cell transfer. Data show mean ± s.dev. and they are representative of two experiments (n=6 per group).

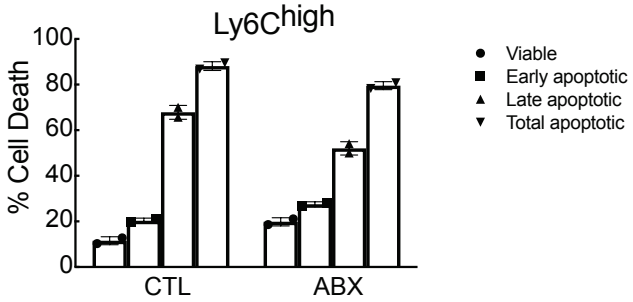

Figure S4. Short antibiotic treatment does not impair splenic Ly6C^{high} monocyte survival *ex vivo.* Related to Figure 3.

FACS-sorted splenic Ly6C^{high} monocytes from mice treated with or without antibiotics for 3 days were stimulated ex vivo with 100 ng/ml LPS. Twenty-four hours later, cells were stained with Annexin V and viability dye eFluor780 to enumerate the frequency of cell death by flow cytometry. Data show the frequency of viable (black bars), early apoptotic (white bars), late apoptotic (blue bars) and total apoptotic cells (red bars) in LPS-stimulated splenic Ly6C^{high} from antibiotic-treated and control animals. Data represent the mean ± s.dev. of technical duplicate wells.

Supplemental Table 1. Relative abundance of taxa significantly reduced during antibiotic treatment. Related to Figure 1

Phylum	Class	Order	Family	Genus	D0	D2	D4
Bacteroidetes	Bacteroidia	Bacteroidales	S24_7	unclassified	40.7%[a]	1.01%	0.49%
Bacteroidetes	Bacteroidia	Bacteroidales	Rikenellaceae	unclassified	20.6%	2.58%	1.14%
Firmicutes	Clostridia	Clostridiales	Clostridiaceae	unclassified	6.5%	8.34%	3.09%
Firmicutes	Clostridia	Clostridiales	Lachnospiraceae	unclassified	3.1%	1.26%	0.33%
Firmicutes	Clostridia	Clostridiales	Ruminococcaceae	Oscillospira	1.8%	1.58%	0.62%
Tenericutes	Mollicutes	RF39	unclassified	unclassified	1.5%	0.44%	0.29%
Firmicutes	Clostridia	Clostridiales	Lachnospiraceae	Coprococcus	0.9%	0.21%	0.03%
Firmicutes	Clostridia	Clostridiales	Ruminococcaceae	Ruminococcus	0.5%	0.16%	0.03%
Firmicutes	Clostridia	Clostridiales	Lachnospiraceae	Roseburia	0.4%	0.00%	0.00%
Firmicutes	Clostridia	Clostridiales	Ruminococcaceae	unclassified	0.3%	0.07%	0.03%
Firmicutes	Clostridia	Clostridiales	Lachnospiraceae	Clostridium piliforme	0.2%	0.00%	0.00%
Firmicutes	Clostridia	Clostridiales	Ruminococcaceae	Anaerotruncus	0.1%	0.03%	0.00%
Firmicutes	Clostridia	Clostridiales	Mogibacteriaceae	unclassified	0.1%	0.03%	0.01%
Firmicutes	Erysipelotrichi	Erysipelotrichales	Erysipelotrichaceae	Allobaculum	0.1%	0.04%	0.01%
Firmicutes	Clostridia	Clostridiales	Lachnospiraceae	Dorea	0.04%	0.01%	0.02%
Firmicutes	Clostridia	Clostridiales	Lachnospiraceae	Anaerostipes	0.04%	0.00%	0.00%
Actinobacteria	Actinobacteria	Bifidobacteriales	Bifidobacteriaceae	Bifidobacterium	0.36%	0.07%	0.22%

[a] Data show mean relative abundance of taxa averaged from eight mice.

Supplemental Table 2. Relative abundance of taxa significantly increased during antibiotic treatment. Related to Figure 1.

Phylum	Class	Order	Family	Genus	D0	D2	D4
Proteobacteria	Betaproteobacteria	Burkholderiales	Alcaligenaceae	Sutterella	0.83%[a]	23.3%	36.7%
Firmicutes	Bacilli	Bacillales	Bacillaceae	Staphylococcus	0	15.4%	17.2%
Verrucomicrobia	Verrucomicrobiae	Verrucomicrobiales	Verrucomicrobiaceae	Akkermansia municiphila	0.35%	5.57%	5.59%
Firmicutes	Bacilli	Lactobacillales	Streptococcaceae	Streptococcus	0	0.26%	2.42%
Firmicutes	Bacilli	Lactobacillales	Enterococcaceae	Enterococcus	0	0.8%	1.72%
Firmicutes	Clostridia	Clostridiales	Lachnospiraceae	Ruminococcus gnavus	0.66%	0.85%	1.64%
Firmicutes	Bacilli	Lactobacillales	Leuconostocaceae	unclassified	0	0.04%	0.8%
Firmicutes	Clostridia	Clostridiales	Peptostreptococcaceae	Peptostreptococcus	0	0.05%	0.54%
Firmicutes	Bacilli	Lactobacillales	unclassified	unclassified	0	0	0.48%
Firmicutes	Bacilli	Bacillales	Bacillaceae	Geobacillus vulcani	0	0.03%	0.4%
Firmicutes	Erysipelotrichi	Erysipelotrichales	Erysipelotrichaceae	Coprobacillus	0.03%	0.1%	0.39%
Firmicutes	Clostridia	Clostridiales	Tissierellaceae	Gallicola	0	0	0.26%
Firmicutes	Clostridia	Clostridiales	Tissierellaceae	Anaerococcus	0	0.03%	0.24%
Actinobacteria	Actinobacteria	Actinomycetales	Sanguibacteraceae	Sanguibacter	0	0	0.13%
Actinobacteria	Actinobacteria	Actinomycetales	Corynebacteriaceae	Corynebacterium	0	0	0.09%
Firmicutes	Bacilli	Bacillales	Paenibacillaceae	Paenibacillus	0	0	0.09%
Proteobacteria	Alphaproteobacteria	Rhizobiales	Rhizobiaceae	Agrobacterium	0	0	0.09%
Firmicutes	Clostridia	Clostridiales	Clostridiaceae	Clostridium	0.1%	0.11%	0.06%
Firmicutes	Bacilli	Bacilllales	unclassified	unclassified	0	0	0.04%
Proteobacteria	Gammaproteobacteria	Enterobacteriales	Enterobacteriaceae	Erwinia	0	0	0.01%

[a] Data show mean relative abundance of taxa averaged from eight mice.

TRANSPARENT METHODS

KEY RESOURCES TABLE

REAGENT or RESOURCE	SOURCE	IDENTIFIER
Antibodies		
Anti-mouse CD3-APC	Biolegend	100236; RRID: AB_2561456
Anti-mouse CD3-PerCP-Cy5.5	Biolegend	100218; RRID: AB_1595492
Anti-mouse B220-APC	Biolegend	103212; RRID: AB_312997
Anti-mouse NK1.1-APC	Biolegend	108710; RRID: AB_313397
Anti-mouse CD49b-APC	Biolegend	108910; RRID: AB_313417
Anti-mouse LY6G-APC	Biolegend	127614; RRID: AB_2227348
Anti-mouse Siglec-F-APC	Miltenyi Biotec	130-102-241; RRID:AB_2653452
Anti-mouse CD11c-BV421	Biolegend	117330; RRID: AB_11219593
Anti-mouse CD11c-BV605	Biolegend	117334; RRID: AB_2562415
Anti-mouse F4/80-BV421	Biolegend	123132; RRID: AB_11203717
Anti-mouse I-A^b-BV421	BD Biosciences	562928; RRID: AB_2737897
Anti-mouse I-A^b-APC/Fire™ 750	Biolegend	116424; RRID: AB_2721487
Anti-mouse CD11b-PeCy7	Biolegend	101216; RRID: AB_312799
Anti-mouse Ly6C-Alexa488	Biolegend	128022; RRID: AB_10639728
Anti-mouse Ly6C-Brilliant Violent 785	Biolegend	128041; RRID: AB_2565852
Anti-mouse Ly6C-PE	Biolegend	128008; RRID: AB_1186132
Anti-mouse CD115-PE	Biolegend	135506; RRID: AB_1937253
Anti-mouse CD45.1-BV711	Biolegend	110739; RRID: AB_1937253
Anti-mouse CD45-BUV395	BD Biosciences	564279; RRID: AB_2651134
Fixable Viability Dye eFluor™ 506	ThermoFisher Scientific	65-0866-18
Fixable Viability Dye eFluor™ 660	ThermoFisher Scientific	65-0864-18
Fixable Viability Dye eFluor™ 780	ThermoFisher Scientific	65-0865-18
Bacterial Strains		
Citrobacter rodentium	ATCC	51459
Escherichia coli, strain K12	The Coli Genetic Stock Center at Yale	CGSC#7296
Cell lines		
HEK-Blue mTLR2	Invivogen	hkb-mtlr2
HEK-Blue mTLR3	Invivogen	hkb-mtlr3
HEK-Blue mTLR4	Invivogen	hkb-mtlr4
HEK-Blue mTLR5	Invivogen	hkb-mtlr5
HEK-Blue mTLR7	Invivogen	hkb-mtlr7
HEK-Blue mTLR9	Invivogen	hkb-mtlr9
HEK-Blue mNOD1	Invivogen	hkb-mnod1
HEK-Blue mNOD2	Invivogen	hkb-mnod2
HEK-Blue Null1	Invivogen	hkb-null1
HEK-Blue Null1-k	Invivogen	hkb-null1k
HEK-Blue Null1-v	Invivogen	hkb-null1v

HEK-Blue Null2	Invivogen	hkb-null2
HEK-Blue Null2-k	Invivogen	hkb-null2k
Chemicals, peptides and enzymes		
Histopaque-1077	Sigma	10771
Ampicillin trihydrate	Sigma	A6140
Buprenorphine SR	Wildlife Pharmaceuticals	https://wildpharm.com/medications/labanimals/item/3-buprenorphine-sr-1ml.html
Meloxicam SR	Wildlife Pharmaceuticals	https://wildpharm.com/meloxicamsr5mllab.html
Metronidazole	Sigma	M1547
Neomycin trisulfate salt hydrate	Sigma	N1876
Vancomycin HCL	Research Products International	V06500-5.0
Gentamicin reagent solution	ThermoFisher Scientific	15750-060
Commercial assays		
eBioscience™ Annexin V Apoptosis Detection Kit APC	ThermoFisher Scientific	88-8007-74
FAM-FLIVO® In vivo Polycaspase Assay	ImmunoChemistry Technologies, LLC	981
Legendplex Mouse Inflammation Panel	Biolegend	740446
Mouse TNF-α Duoset ELISA kit	R&D Systems	DY410-05
Mouse IL-6 Duoset ELISA kit	R&D Systems	DY406-05
Mouse IL-10 Duoset ELISA kit	R&D Systems	DY417-05
Mouse IL-1α/IL-1F1 Duoset ELISA kit	R&D Systems	DY400-05
Mouse IL-1β/IL-1F2 Duoset ELISA kit	R&D Systems	DY401-05
PRR ligands		
Pam2CSK4	Invivogen	tlrl-pm2s-1
Poly (I:C) HMW	Invivogen	tlrl-pic
LPS, *E.coli* O55:B5	Sigma	L4524
FLA-ST	Invivogen	tlrl-stfla
CL264	Invivogen	tlrl-c264e-5
ODN1826	Invivogen	tlrl-1826-1
iE-DAP	Invivogen	tlrl-dap
MDP	Invivogen	tlrl-mdp
Software		
FlowJo v.10.5.3.	FlowJo, LLC	https://www.flowjo.com
BioRender		Biorender.com
GraphPad Prism v.8.2.0.	Prism-graphpad.com	https://www.graphpad.com/scientific-software/prism/
Metacore	Clarivate Analytics	https://portal.genego.com/
LefSE		https://huttenhower.sph.harvard.edu/galaxy/

QIIME		https://view.qiime2.org/
Taqman Probes		
Mouse *IL-1α*	Applied Biosystems	Mm00439620_m1
Mouse *IL-1β*	Applied Biosystems	Mm00434228_m1
Mouse *IL-6*	Applied Biosystems	Mm00446190_m1
Mouse *IL-10*	Applied Biosystems	Mm01288386_m1
Mouse *TNF-α*	Applied Biosystems	Mm00443258_m1
Mouse *Trem1*	Applied Biosystems	Mm01278455_m1
Mouse *S100a8*	Applied Biosystems	Mm00496696_g1
Mouse *S100a9*	Applied Biosystems	Mm00656925_m1
Mouse *CD36*	Applied Biosystems	Mm00432403_m1
Mouse *Camp*	Applied Biosystems	Mm00438285_m1
Mouse *Ciita*	Applied Biosystems	Mm00482914_m1
Mouse *Gapdh*	Applied Biosystems	Mm99999915_g1
Others		
Fluoresbrite® Yellow Green Microspheres, 0.5 micrometer	Polysciences, Inc	17152-10
Deposited data	Mendeley data	http://dx.doi.org/10.17632/tjdwjnzskr.1

Animals

Female C57BL/6 (stock number 000664) and B6 CD45.1 (stock number 002014) mice were purchased from The Jackson Laboratory and were used at 6-8 weeks of age. All animals were kept in a pathogen-free facility at Brigham and Women's Hospital (BWH) in accordance with the animal protocol guidelines prescribed by the Institutional Animal Care and Use Committee of BWH. Germ-free C57BL/6 mice were bred and raised in gnotobiotic isolators at Massachusetts Host-Microbiome Center at BWH. Mice were housed in at least two cages per group to minimize cage-related effects.

Antibiotic treatment

SPF and GF mice were treated with a broad-spectrum antibiotic cocktail consisting of vancomycin (0.5 g/L), ampicillin (1 g/L), neomycin (1 g/L) and metronizadole (1g/L) dissolved in drinking water. SPF mice received the antibiotic-containing water *ad libitum* for

2-6 days in all experiments. The antibiotic cocktail was administered by oral gavage for 4 days only in GF and control SPF animals to avoid signs of dehydration seen in GF mice treated with antibiotic-containing water *ad libitum*. All antibiotics were purchased from Sigma except vancomycin (Research Products International).

Preparation of single-cell suspensions from blood, spleen and bone marrow.

Blood was isolated from the facial vein of mice using a 5 mm goldenrod lancet (VWR) and collected in BD Microtainer tubes with lithium heparin (Becton Dickinson). Heparinized-blood was loaded onto Histopaque-1077 (Sigma) and centrifuged for 20 minutes at 900 x g, at 25° C. The interphase containing blood mononuclear cells was collected and stained for monocyte subsets. Single-cell suspensions from spleens were prepared by mechanical disruption using a 70-μm-cell strainer/nylon mesh (Fisher Scientific). Perfusion was not performed before isolation of spleens as the number of contaminating blood monocytes is negligible (Swirski et al., 2009). Bone marrow cells were isolated from both femurs and tibias of animals after centrifugation of bones at 14,000 rpm for 15 seconds. Red blood cells were eliminated from splenic and bone marrow cell suspensions using the ACK lysing buffer (Lonza). Viability and total cell numbers were determined upon staining with Trypan Blue (GE Healthcare Life Sciences) using a hemocytometer.

Flow cytometry and cell-sorting

Single-cell suspensions from blood, spleen and bone marrow were stained with an anti-CD16/32 antibody (BioXCell) to block Fc receptors for 15 minutes on ice. Afterwards, the antibodies described in Key Resources Table were used to stain cell suspesions. Live

monocytes were identified as CD11b^{high} LIN (eFluor660, CD3, B220, NK1.1, CD49b, Ly6G, Siglec-F)$^{-}$ (F4/80, CD11c, I-Ab)^{low} and Ly6C^{high}. Macrophages/dendritic cells were identified as CD11b^{high} LIN (eFluor660, CD3, B220, NK1.1, CD49b, Ly6G, Siglec-F)$^{-}$ (F4/80, CD11c, I-Ab)^{high} and Ly6C^{low}. Monocytes/macrophages/dendritic cell numbers were calculated by multiplying the number of total cells with the percent of the respective gate. To calculate the absolute cell number within the splenic tissue, total monocyte number was normalized to weight (mg) of spleen. Data were acquired on a BD LSRII and BD LSRFortessa (BD Biosciences) and analyzed with FlowJo v.10.5.3. (FlowJo, LLC). For cell sorting, splenic and bone marrow suspensions were pre-enriched in CD11b^{+} cells using the CD11b Microbeads (Miltenyi Biotec) and then stained with the antibodies for sorting. Cells were sorted in a BD FACSAria II (BD Biosciences) using a 100 µm nozzle at 20 psi.

Quantitative real-time PCR (Q-PCR)

FACS-sorted splenic Ly6C^{high} monocytes were lysed in RLT buffer and RNA was extracted using the RNeasy® Micro Kit (Qiagen) according to the manufacturer's instructions. cDNA was synthesized by the High Capacity cDNA Reverse Transcription kit (Applied Biosystems). qPCR was performed using Taqman Universal PCR Master Mix and Taqman Gene Expression Assays (Applied Biosystems) in technical duplicate wells. All primers and probes were from Applied Biosystems as described in Key Resources Table. All assays were performed using a ViiA7 system (Applied Biosystems). Results were normalized to the housekeeping gene *Gapdh*. The relative expression of each target gene was expressed as ($2^{-\Delta Ct}$) (Livak et al., 2001), where ΔCt is the difference between the mean Ct of the target gene and the mean Ct of *Gapdh*. Gene expression of *Gapdh* was stable between the

antibiotic-treated and control groups.

nCounter gene expression and analysis

FACS-sorted splenic Ly6C^{high} monocytes from experimental and control groups were lysed in RLT buffer and cell lysates were hybridized with reporter and capture probes for nCounter Gene Expression code sets (Mouse Immunology Panel), according to the manufacturer's instructions (Nanostring Technologies). Analysis of expression of 561 genes was performed using the nSolver analysis software, version 4.0.62 (Nanostring Technologies). Data were normalized to spiked positive controls and housekeeping genes. Transcript counts less than 50 were excluded from the analysis as they were considered as background.

Metacore analysis

Data were analyzed using the Metacore software. Differentially expressed genes (with corresponding fold-changes and p values) were uploaded and analyzed by the Enrichment Analysis Tool as well as the Interactome Tool to generate biological networks and predict the top ten transcription factors involved in the regulation of the differentially expressed genes.

Adoptive transfer of splenic monocytes

Splenic Ly6C^{high} monocytes were transferred to recipient mice intrasplenically. Recipient CD45.2 mice were administered water with or without antibiotics for 3 days. Before cell transfer, recipient mice were s.c. injected with 0.6 mg/kg buprenorphine SR and 4 mg/kg

meloxicam SR solutions to minimize post-operative pain (both from Wildlife Pharmaceuticals) and shaved on the middle left side of the abdomen. Then, a skin incision between the last rib and hip joint was made and 5 x 10^4 FACS-sorted splenic Ly6C^{high} monocytes from CD45.1 mice, resuspended in 20 µl sterile PBS, were injected in the subcapsular layer of the spleens of CD45.2 mice. Next, the tissue was sutured using 4.0 chromic gut absorbable sutures. Six hours after the transfer, cell suspensions from blood and spleens of the recipient mice were prepared, stained for the presence of CD45.1$^+$ monocytes and analyzed by flow cytometry.

In vivo phagocytosis

Mice were treated with or without antibiotics for three days. On day three, animals underwent the surgical process described above. Once, spleen was exteriorized, we injected 20 µl of Fluoresbrite Yellow Green Microspheres (0.5 µm; Polysciences) per mouse. Next, the tissue was sutured using 4.0 chromic gut absorbable sutures. Twenty-four hours later, splenic single-cell suspensions were prepared and the frequency of fluorescently labeled splenic Ly6C^{high} monocytes was quantified by flow cytometry.

Detection of cell death *ex vivo*

FACS-sorted splenic Ly6C^{high} monocytes were stimulated with 100 ng/ml LPS for 24 hours. Then, cells were stained with the eBioscience Annexin V apoptosis detection kit and eBioscience Fixable viability dye eFluor780 (all from ThermoFisher Scientific), according to the manufacturer's instructions. Early apoptotic cells were considered as Annexin V$^+$ eFluor780$^-$ whereas late apoptotic cells were Annexin V$^+$ eFluor780$^+$. Necrotic cells,

Annexin V^- $eFluor780^+$, were not detected. For determining the apoptotic rate of monocytes from antibiotic-treated mice, animals were administered water with or without antibiotics for 3 days. On day 3, splenic cell suspensions were incubated with FAM-FLIVO for 60 minutes at 37° C for 60 minutes. Cells were washed twice, fixed and analyzed by flow cytometry.

Ligand injections

Naïve mice were administered water with or without antibiotics for three days. One and two days after initiation of the antibiotic treatment, mice were injected i.p. with ie-DAP (25 µg/mouse) or MDP (25 µg/mouse). Another group of mice received a TLR ligand cocktail consisting of Pam2CSK4 (5 µg/mouse), LPS (5 µg/mouse), CL264 (5 µg/mouse), ODN1826 (5 µg/mouse) and FLAST (1 µg/mouse) only once, one day after initiation of the antibiotics.

Gentamicin Protection assay

FACS-sorted splenic $Ly6C^{high}$ monocytes were incubated for 2 hours with *C.rodentium* or *E.coli*, K12 strain, at a multiplicity of infection (MOI) of 20. Next, cells were washed to remove extracellular bacteria and further treated with gentamicin for 1 hour. Then, supernatant was collected to ensure the absence of live extracellular bacteria within the wells and cells were lysed in 1% triton buffer. Serial dilutions of the cell lysates and supernatants were plated on agar plates in triplicates and the number of colonies was counted after overnight incubation at 37° C. Results are presented as absolute CFU counts.

Detection of cytokines in the supernatant

FACS-sorted splenic Ly6C^{high} monocytes from antibiotic-treated and untreated mice were stimulated with or without 100 ng/ml LPS (from E. coli O55:B5, Sigma) for 24 hours. Cell-free culture supernatants were examined for the presence of cytokines using the Legendplex Mouse Inflammation Panel (Biolegend). Quantification of TNF-α, IL-6, IL-1α, IL-1β and IL-10 in samples was also assessed by ELISA kits (DuoSet Kits, R&D Systems), according to the manufacturer's instructions.

Detection of bacterial products in murine sera

C57BL/6 mice were treated with or without antibiotics for 4 days and sera were isolated from both groups before as well as 2 and 4 days after initiation of the treatment. To assess the presence of bacterial products, sera from all time points were incubated with the HEK-Blue TLR2, TLR3, TLR4, TLR5, TLR7, TLR9, NOD1, NOD2 as well as the control cell lines which lack the corresponding PRR (all from Invivogen). Briefly, HEK293 cells stably co-express murine TLRs and an NF-κB/AP-1 inducible SEAP (secreted embryonic alkaline phosphatase) reporter gene. In the presence of TLR agonists, activation of NF-κB/AP-1 leads to SEAP secretion in the cell supernatant. Addition of a specific SEAP color substrate in the wells produces a purple/blue color that was measured at 620 nm using a microplate reader. The HEK-Blue cell lines were incubated with HEK-Blue detection medium for sixteen hours before measuring the O.D., according to the manufacturer's instructions.

Microbial Quantification by qPCR

Bacterial DNA was extracted from fecal samples using the DNeasy Powerlyzer PowerSoil kit (Qiagen), according to the manufacturer's instructions. qPCR analysis was performed in duplicate wells by Taqman amplification reactions consisting of genomic DNA, Taqman® Universal PCR Master Mix (Applied Biosystems) and the following primer pair: Forward primer: TCCTACGGGAGGCAGCAGT, Reverse primer: GGACTACCAGGGTATCTAATCCTGTT, Probe (FAM): CGTATTACCGCGGCTGCTGGCAC (Nadkarni et al., 2002). Relative expression of the 16S gene was calculated based on the expression of the gene before treatment in each mouse. Relative expression was normalized to mg of fecal sample.

16s rRNA sequencing and taxonomic microbiota analysis

Fecal DNA was isolated as described above. Amplicons spanning variable region 4 (V4) of the 16S rRNA gene were generated with barcode containing primers and sequenced on Illumina MiSeq. Data processing was performed using an established protocol (Caporaso et al., 2010) using the Qiime software (version 2018.11). Shannon's index and observed OTUs were used to measure alpha diversity whereas beta diversity was expressed as weighted and unweighted UniFrac distance. A Principal coordinates analysis (PCoA) plot was generated to visualize the similarity of the community members. The LefSe algorithm (Segata et al., 2011) was used to identify differentially abundant features that are statistically different among different groups.

QUANTIFICATION AND STATISTICAL ANALYSIS

Statistical data analysis was performed with Prism software version 8.0 (GraphPad Software). For comparisons of two groups, two-tailed Student's t-test was used. Comparisons of multiple groups were made using one-way ANOVA, as described in the figure legends. Data represent mean ± standard error of the mean (SEM) or mean ± standard deviation (s.dev.), as indicated in the figure legend. $P < 0.05$ was considered significant.

SUPPLEMENTAL REFERENCES

Swirski, F.K. et al., 2009. Identification of splenic reservoir monocytes and their deployment to inflammatory sites. *Science (New York, N.Y.)*, 325(5940), pp.612–616.

Livak, K.J. et al., 2001. Analysis of relative gene expression data using real-time quantitative PCR and the $2^{-\Delta\Delta C}_T$ method. *Methods*, 25, pp.402-408.

Caporaso, J.G. et al., 2010. QIIME allows analysis of high-throughput community sequencing data. *Nature methods*, 7(5), pp.335–336.

Nadkarni, M.A. et al., 2002. Determination of bacterial load by real-time PCR using a broad-range (universal) probe and primers set. *Microbiology (Reading, England)*, 148(Pt 1), pp.257–266.

Segata, N. et al., 2011. Metagenomic biomarker discovery and explanation. *Genome biology*, 12(6), p.R60.